Rapid Communications

Imaging of polarization-sensitive metasurfaces with quantum entanglement

Charles Altuzarra,[1,*] Ashley Lyons,[2,*] Guanghui Yuan,[3,*] Christy Simpson,[2] Thomas Roger,[4]
Jonathan S. Ben-Benjamin,[1] and Daniele Faccio[2,†]
[1]*Texas A&M University, College Station, Texas 77843-4242, USA*
[2]*School of Physics & Astronomy, University of Glasgow, Glasgow G12 8QQ, United Kingdom*
[3]*Centre for Disruptive Photonic Technologies, TPI, Nanyang Technological University, Singapore 637371, Singapore*
[4]*Institute of Photonics and Quantum Sciences, Heriot-Watt University, Edinburgh EH14 4AS, United Kingdom*

(Received 8 October 2018; published 7 February 2019)

Quantum entanglement is a key resource that can be exploited for a range of applications such as quantum teleportation, quantum computation, and quantum cryptography. However, efforts to exploit entanglement in imaging systems have so far led to solutions such as ghost imaging, that have since found classical implementations. Here, we demonstrate an optical imaging protocol that relies uniquely on entanglement: Two polarizing patterns imprinted and superimposed on a metasurface are separately imaged only when using entangled photons. Unentangled light is not able to distinguish between the two patterns. Entangled single-photon imaging of functional metasurfaces promises advances towards the use of nanostructured subwavelength thin devices in quantum information protocols and a route to efficient quantum state tomography.

DOI: 10.1103/PhysRevA.99.020101

Introduction. Quantum imaging has yielded many advantages including enhancement of spatial resolution beyond the diffraction limit [1,2], sub-shot-noise imaging [3,4], ghost imaging [5–9], and the ability to image with photons that are never detected [10]. Of particular interest to this study are imaging techniques whereby an image can only be obtained with one photon when a nonlocal measurement is performed on another, namely, ghost imaging, and works concerning the imaging of undetected photons. Both these techniques were originally demonstrated with quantum entangled pairs of photons, and indeed the first impression was that these techniques relied on the unique properties of quantum entanglement and specifically on the nonlocal nature of entanglement that allows for control of a measurement through another measurement performed at a different place and time. However, both of these procedures have since been shown to only depend on correlation measurements that are also possible with classical states of light [11–13]. Take, as an example, ghost imaging, which is a procedure where an image is formed using a detector that records no spatial information (i.e., a bucket detector) by evaluating the correlations between the bucket detector measurement and a second spatially resolved measurement. Where previously it was thought that this could only be achieved with pairs of photons entangled in the spatial domain, the two photons in fact are only required to share some spatial correlation. Nevertheless, in particular, with reference to ghost imaging, these quantum-inspired techniques have led to a variety of novel imaging methods [14–17].

Metamaterials and their two-dimensional counterparts, metasurfaces, have recently started to emerge as a platform that is viable for quantum processing at the single-photon level. The first pioneering works demonstrated that quantum entanglement could be preserved in transmission through a metasurface [18], followed by evidence that photon indistinguishability could be preserved in passing from photons to plasmons, thus allowing one to perform simple quantum processing steps such as Hong-Ou-Mandel bunching experiments directly on plasmonic chips [19]. Recent experiments have also highlighted how the losses associated with metasurfaces may be harnessed as a resource [20,21] to thus control the transmitted photon statistics [22–24].

Recent advances in metasurface optical design have provided ultrathin devices that are capable of controlling and shaping the optical properties of a light beam, for example, polarization, orbital angular momentum (OAM), and focusing. More complex devices are also possible whereby the output depends on the input properties, for example, the output OAM or an output holographic image can be controlled by varying the input polarization [25–27]. These approaches have also very recently been extended to the quantum regime, showing generation and control of entanglement at the metasurface [28,29].

In the following Rapid Communication, we introduce a quantum imaging protocol that fundamentally depends on nonclassical photon correlations where images are formed only in the presence of entanglement. We show that single photons transmitted through a polarization-sensitive metasurface imprinted with two different patterns can produce clear images (either a star or a triangle) only when a corresponding measurement is performed on its polarization-entangled partner photon. Conversely, in cases where entanglement is not present, a composite image is observed (the sum of both the star and triangle) regardless of any postselection on the photons. Moreover, in general, degrading the photon pair entanglement degrades the quality of the image.

*These authors contributed equally to this work.
†daniele.faccio@glasgow.ac.uk

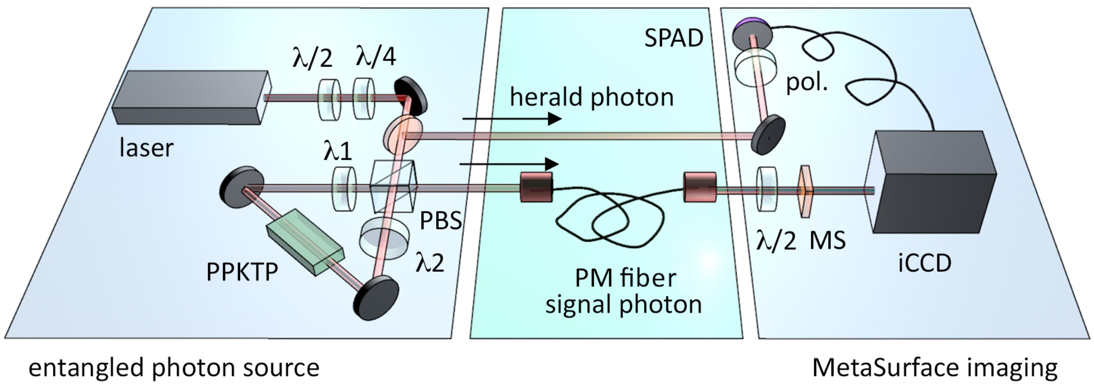

FIG. 1. Polarization-entangled imaging with metasurfaces. Entangled photon pairs are generated within a PPKTP nonlinear crystal surrounded by a Sagnac loop such that it is pumped by two counterpropagating pump beams (controlled by quarter- and half-wave plates) from a 404-nm cw laser. Two wave plates (λ1 and λ2) rotate the polarizations of the pump and SPDC photons, respectively, for one direction around the Sagnac loop. At the polarizing beam splitter (PBS), one photon (the herald) is directed to a polarizer (pol.) while the other (signal) is transmitted through the polarization-sensitive plasmonic metasurface (MS) and detected on an iCCD camera. Before the metasurface, we insert an fiber optical delay line so that the photon arrives on the iCCD when the camera electronic shutter is activated by the herald photon trigger. A half-wave plate placed in front of the metasurface is used to rotate the photon polarization state by 45° that is equivalent to rotating the metasurface by 45°. Light is focused onto the metasurface and then imaged onto the iCCD using microscope objectives (not shown in the figure)

Experiment. The experimental setup is shown in Fig. 1. We generated pairs of photons with orthogonal polarizations at a wavelength of 808 nm by spontaneous parametric down-conversion (SPDC) in a type-II periodically poled potassium titanyl phosphate (PPKTP) nonlinear crystal that was pumped by a continuous-wave 100-mW laser at 404-nm wavelength. The polarization-entangled state is generated using a counterpropagating Sagnac interferometer enclosing the PPKTP crystal [30,31]. The input 404-nm pump laser beam polarization is fully controlled by $\lambda/4$ and $\lambda/2$ wave plates and is split into two counterpropagating beams at the polarization beam splitter (PBS). Two-wavelength wave plates rotate the polarization of the pump, without affecting the SPDC photon polarization (indicated as $\lambda 1$) and of the SPDC photons, without affecting the pump polarization (indicated as $\lambda 2$). We label photons propagating in the two output modes of the PBS *herald* (upwards) and *signal* (right). The Sagnac interferometer thus produces an entangled output state from the PBS of the form $|H_hV_s\rangle + |V_hH_s\rangle$, where the subscripts (h, s) denote the herald and signal photons, respectively. The herald photon is detected with a single-photon avalanche diode (SPAD), the output of which was connected to the external trigger of an intensified-CCD camera (iCCD, ANDOR iStar) and thus heralds the arrival of a photon at the camera sensor. The second photon of the pair, the signal photon, was optically delayed by 40 m of optical fiber (in order to compensate for the electronic delay acquired by the iCCD camera between the trigger arrival and the actual acquisition on the iCCD sensor) before being focused onto the metasurface sample and imaged onto the iCCD sensor by a pair of $\times 10$ objective lenses (not shown for simplicity in Fig. 1).

In Fig. 2 we show the metasurface that has two different patterns, a star and a triangle, that also act as polarizers, i.e., they only transmit horizontally and vertically polarized light, respectively.

Quantum metasurface theory. In our experiment, we produce photon pairs in two states, a mixed state and a pure state. We produce the mixed state $\hat{\rho}_{\text{mixed}}$,

$$\hat{\rho}_{\text{mixed}} = \tfrac{1}{2}|H_hV_s\rangle\langle H_hV_s| + \tfrac{1}{2}|V_hH_s\rangle\langle V_hH_s|, \tag{1}$$

where the herald photon, denoted by a subscript h, travels to the SPAD, and the signal photon, denoted by a subscript s, travels to the iCCD. See Fig. 1. With classical probabilities $\frac{1}{2}$ for the two terms, we produce the pure state $\hat{\rho}_{\text{pure}}$,

$$\begin{aligned}\hat{\rho}_{\text{pure}} &= \tfrac{1}{2}(|H_hV_s\rangle - |V_hH_s\rangle)(\langle H_hV_s| - \langle V_hH_s|)\\ &= \tfrac{1}{2}(|H_hV_s\rangle\langle H_hV_s| - |H_hV_s\rangle\langle V_hH_s|\\ &\quad - |V_hH_s\rangle\langle H_hV_s| + |V_hH_s\rangle\langle V_hH_s|),\end{aligned} \tag{2}$$

where we have the same probability amplitude of the signal and herald photons being in the HV state as vice versa, where

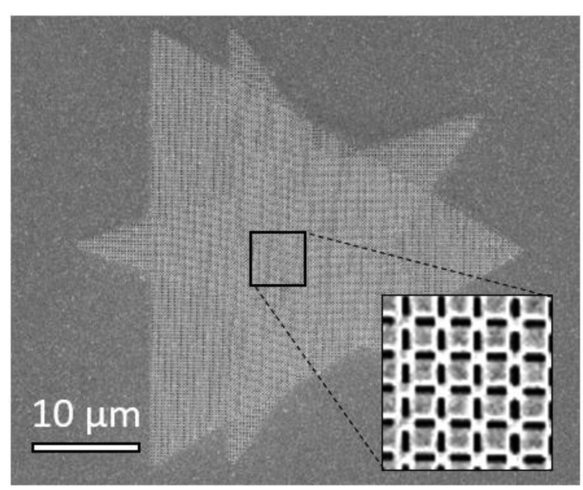

FIG. 2. Metasurface: An image of the metasurface used in the experiments. The two overlaid patterns can be clearly observed: The triangle pattern transmits only horizontally polarized light and the star transmits only vertically polarized light.

H and V stand for the horizontal and vertical polarization states of the photon, respectively. In addition, we actually also produce states in which both photons reach the iCCD, and others, where both go to the SPAD; however, our measuring scheme naturally selects the subensemble excluding those, since they do not yield coincidence counts. To model the heralding of a herald photon with a polarizer at some angle ϕ, we multiply the density matrix with the polarization projection operator $\hat{\chi}$ and perform a partial trace over the herald photon,

$$\begin{aligned}\hat{\chi}_h(\phi) &= |\phi\rangle\langle\phi| \\ &= (\cos\phi|V_h\rangle + \sin\phi|H_h\rangle)(\cos\phi\langle V_h| + \sin\phi\langle H_h|) \\ &= \cos^2\phi|V_h\rangle\langle V_h| + \cos\phi\sin\phi|V_h\rangle\langle H_h| \\ &\quad + \cos\phi\sin\phi|H_h\rangle\langle V_h| + \sin^2\phi|H_h\rangle\langle H_h|. \end{aligned} \tag{3}$$

Heralding a photon. After heralding a photon through a polarizer at some angle ϕ, the (unnormalized) state $\hat{\rho}^{(s)}$ of the signal photon impinging on the metasurface becomes (for our two states, $\hat{\rho}_{\text{mixed}}$ and $\hat{\rho}_{\text{pure}}$)

$$\begin{aligned}\hat{\rho}^{(s)}_{\text{mixed}} &= \text{Tr}_h\{(\hat{\chi}_\phi \otimes \hat{1}_s)\hat{\rho}_{\text{mixed}}\} \\ &= \tfrac{1}{2}\cos^2\phi|H\rangle\langle H| + \tfrac{1}{2}\sin^2\phi|V\rangle\langle V|,\end{aligned} \tag{4}$$

$$\begin{aligned}\hat{\rho}^{(s)}_{\text{pure}} &= \text{Tr}_h\{(\hat{\chi}_\phi \otimes \hat{1}_s)\hat{\rho}_{\text{pure}}\} \\ &= \tfrac{1}{2}(\sin\phi|V\rangle - \cos\phi|H\rangle)(\sin\phi\langle V| - \cos\phi\langle H|),\end{aligned} \tag{5}$$

where we omitted the s subscripts since at this level we have no herald photon and we only have a signal photon.

Passage through metasurface. We model the passage through the metasurface oriented along the angle ξ by the operator

$$\hat{M} = \vartheta_\blacktriangle(\xi)\hat{\chi}_s(\xi) + \vartheta_\bigstar(\xi)\hat{\chi}_s(\xi + 90^\circ), \tag{6}$$

where $\vartheta_\blacktriangle(\xi)$ and $\vartheta_\bigstar(\xi)$ are the position- and polarization-dependent transmission amplitude coefficients of the metasurface for the triangle and star, respectively, when the metasurface is orientated at the angle ξ. See Fig. 2. Considering only the ▲ part (the star part will follow along the same lines), we find that the photon intensity passing through the metasurface is (for our two states, mixed and pure)

$$\begin{aligned}O^\blacktriangle_{\text{mixed}} &= \vartheta_\blacktriangle(\xi)\text{Tr}\{\hat{\chi}_\xi\, \hat{\rho}^{(s)}_{\text{mixed}}\} \\ &= \tfrac{1}{2}\vartheta_\blacktriangle(\xi)[\cos^2\phi\sin^2\xi + \sin^2\phi\cos^2\xi],\end{aligned} \tag{7}$$

$$\begin{aligned}O^\blacktriangle_{\text{pure}} &= \vartheta_\blacktriangle(\xi)\text{Tr}\{\hat{\chi}_\xi\, \hat{\rho}^{(s)}_{\text{pure}}\} \\ &= \tfrac{1}{2}\vartheta_\blacktriangle(\xi)[\sin^2\xi\cos^2\phi \\ &\quad - 2\cos\xi\sin\xi\cos\phi\sin\phi + \cos^2\xi\sin^2\phi].\end{aligned} \tag{8}$$

The expectation value of the final measurement (i.e., the image that is observed on the iCCD camera) is given by $\langle O\rangle = \text{Tr}[\hat{\rho}\,\hat{\chi}_h(\phi)\hat{M}(\xi)]$, where ϕ is the herald photon polarizer angle, which can be nonlocally controlled by the measurement process on the "herald" arm of the experiment. Similarly, to

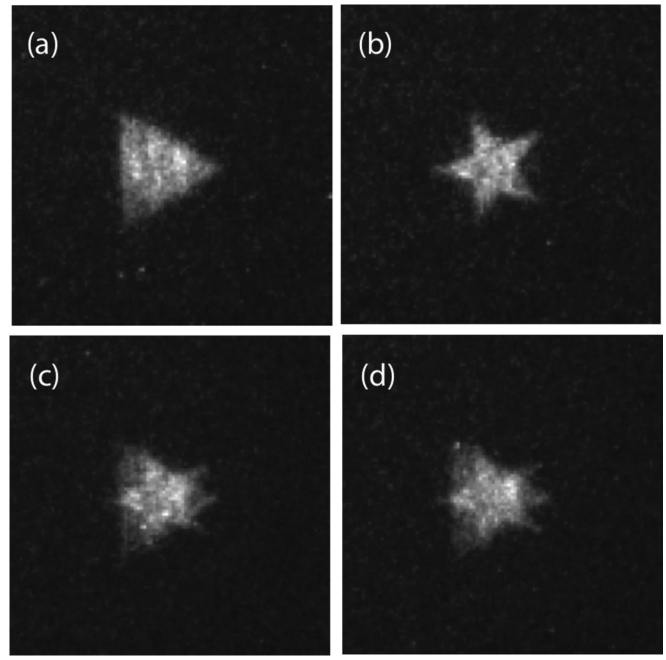

FIG. 3. Imaging with entangled photons: Images obtained with entangled states (measured Bell parameter $S = 2.5$) with the herald polarizer selecting photons at (a) 45° and (b) 135°. The same images obtained with a mixed state (measured Bell parameter $S = 1.6$) at (c) 45° and (d) 135°.

Eqs. (7) and (8), the intensity of a signal photon transmitted through a pixel in the ★ region of the metasurface is

$$O^\bigstar_{\text{mixed}} = \tfrac{1}{2}\vartheta_\bigstar(\xi)[\cos^2\phi\cos^2\xi + \sin^2\phi\sin^2\xi], \tag{9}$$

$$\begin{aligned}O^\bigstar_{\text{pure}} &= \tfrac{1}{2}\vartheta_\bigstar(\xi)[\cos^2\phi\cos^2\xi \\ &\quad + 2\cos\phi\sin\phi\cos\xi\sin\xi + \sin^2\phi\sin^2\xi].\end{aligned} \tag{10}$$

To define a visibility, we integrate over the position and normalize the total areas of our signals from both the ★ and ▲ regions. The visibility is

$$V = \frac{O^\blacktriangle - O^\bigstar}{O^\blacktriangle + O^\bigstar}, \tag{11}$$

and using that $O^\blacktriangle_{\text{mixed}} + O^\bigstar_{\text{mixed}} = 1/2$ and that $O^\blacktriangle_{\text{pure}} + O^\bigstar_{\text{pure}} = 1/2$, we find that the visibilities are

$$V_{\text{mixed}} = (2\cos^2\phi - 1)(2\sin^2\xi - 1), \tag{12}$$

and

$$V_{\text{pure}} = V_{\text{mixed}} - \sin(2\phi)\sin(2\xi). \tag{13}$$

Equations (12) and (13) are confirmed by our experiments. See Fig. 3, where we present the following special cases. Orienting the metasurface at 45°, we find that the visibility of the mixed state is constant (zero), and the visibility of the pure state is $-\sin(2\phi)$. When we orient the metasurface to 0°, we find that both the pure- and mixed-state visibilities are the same, $-\cos(2\phi)$. Calculation of the expectation value $\langle O\rangle$ reveals that for a mixed (not entangled) state, we will always see a superposition of both the polarization-dependent patterns, i.e., a superposition of a star and a triangle. However, in the presence of a pure quantum state of the form $|\Psi\rangle$, imaging only in the presence of a D (or AD) herald photon will selectively image only the AD (or D) metasurface pattern, i.e., the star or triangle alone will become clearly visible without any overlap of the other. Figures 3(a) and 3(b) show the experimental measurements obtained for entangled photons, when selecting D and AD herald photons, respectively. We separately measured the Bell parameter for the photon state used in this experiment to be $S = 2.5$ (i.e., above the threshold $S = 2$ for entanglement and close to the maximally entangled value of $S = 2\sqrt{2}$): The triangle and star are individually very clearly visible, with high contrast and no visible contribution of the other shape. The Sagnac interferometer can also be used to produce a mixed polarization state by rotating the $\lambda 2$ wave plate to 0° such that the PPKTP crystal is pumped in both directions around the Sagnac loop but there is no compensation for the SPDC-photon temporal walk-off occurring within the crystal.

Entangled state imaging of metasurface structures. Using the experimental layout shown in Fig. 1, we generate an entangled state described by Eq. (2). We place the metasurface in the optical path of the signal photons with a polarization axis orientated at 45° to the polarization of the photons. The state has the form

$$\hat{\rho} = \tfrac{1}{2}(|H_hV_s\rangle\langle H_hV_s| + |V_hH_s\rangle\langle V_hH_s|). \tag{14}$$

In this way, the experiment can be repeated with nonentangled photons with a Bell parameter that was measured to be $S = 1.6$. The results are shown in Figs. 3(c) and 3(d), that look nearly identical regardless of the herald photon polarization and show a clear superposition of both the star and triangle. Figure 4 shows the full results for these measurements (i.e., for varying angles of the selected herald photon polarization from 0° to 360° with a direct comparison to the theoretical predictions [32]). In particular, we measure the visibility of the "triangle" image, $V = (O_\blacktriangle - O_\bigstar)/(O_\blacktriangle + O_\bigstar)$. One could use the signal-to-noise ratio as a possible figure of merit. Here, we prefer to use the image visibility as this allows us to also make a direct connection to the Bell inequality tests (see below). For the case when the metasurface is aligned with the H-V axis of the input photons ($\xi = 0°$), the theory predicts $V_{\text{pure}} = V_{\text{mixed}} = -\cos(2\phi)$. Alternatively, for the more interesting case in which the metasurface angle $\xi = 45°$, we predict

$$V_{\text{mixed}} = 0 \quad \text{and} \quad V_{\text{pure}} = -\sin(2\phi) \tag{15}$$

for the mixed and pure states, respectively. As can be seen in Fig. 4, there is a good agreement between the experiment and theory, although the visibility is lower in the experiment due to background noise on the iCCD sensor. Nevertheless, the main features are clearly observable: Figs. 4(a) and 4(b) show the case in which the metasurface is aligned parallel to the H-V polarization of the photons. The image intensities are essentially identical for the cases of input mixed and pure states, i.e., there is no discernible advantage or difference using entangled states. Conversely, Figs. 4(c) and 4(d) show the case in which the metasurface is aligned at 45° to the H-V polarization of the photons: Now the unentangled state shows zero visibility whereas imaging with entangled photons gives rise to clear oscillations in the triangle visibility. Each peak corresponds to all photons being in the triangle image and none in the star image and each trough corresponds to the opposite situation.

In Fig. 5 we show image visibility for the triangle as we gradually increase the degree of entanglement (increasing the Bell parameter S). The experimental points are shown

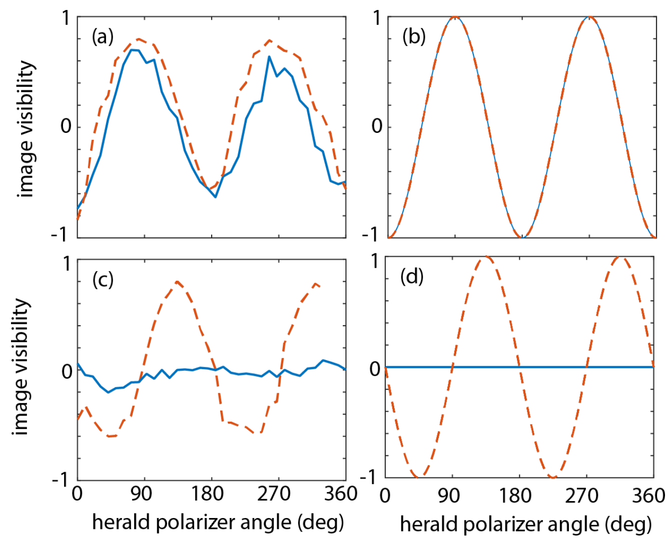

FIG. 4. Imaging with entangled photons: Image visibility, $V = (O_\blacktriangle - O_\bigstar)/(O_\blacktriangle + O_\bigstar)$, for the triangle image plotted vs the herald photon polarizer angle. (a) Experimental and (b) theoretical results for the case of the metasurface aligned along the H-V axis of the input photons. (c) Experimental and (d) theoretical results for the case of the metasurface aligned at 45° with respect to the polarization of the input photons. In all figures, solid lines refer to an input mixed state and dashed lines refer to input pure states with a measured Bell parameter $S = 2.5$.

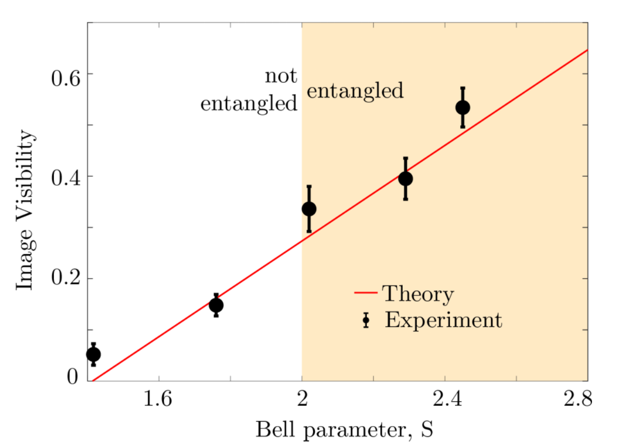

FIG. 5. Imaging with entangled photons: Image visibility for the triangle image plotted vs the herald photon polarizer angle for increasing degree of entanglement as measured by the Bell parameter S. The experimental points show the visibility $V = (O_\blacktriangle - O_\bigstar)/(O_\blacktriangle + O_\bigstar)$ and the theory curve is calculated as $V = (O_\blacktriangle - O_\bigstar)/(O_\blacktriangle + O_\bigstar + 2\sigma)$, where σ accounts for background noise on the detector that was measured to be 12% of the maximum measured signal.

as points with error bars (95% confidence bound of the sinusoidal fits to the curves shown, e.g., in Fig. 4). The solid line shows the theoretical prediction based on the model described above accounting also for the detector noise σ that was measured to be of order of 200 counts ($\sim$10% of the maximum measured photocounts in the image area), i.e., $V = (O_\blacktriangle - O_\bigstar)/(O_\blacktriangle + O_\bigstar + 2\sigma)$. The data follow the theoretical expectation and highlight how the image visibility depends the degree of entanglement, dropping to zero for correlated but unentangled photon pairs and reaching maximum visibility for $S = 2\sqrt{2}$ that is limited only by the noise on the camera.

Conclusions. We have demonstrated an imaging protocol that is inherently dependent on the nonlocal and superposition properties between a pair of entangled photons. With input states that are entangled and *under the assumption of only H and V photon illumination*, it is possible to clearly distinguish the individual images imprinted on the metasurface, i.e., individual images become visible only in the presence of pure, entangled states. This functionality is the result of quantum interference occurring on the metasurface, in line with recent reports of "quantum metamaterials" [28,29].

The wavelength dependence of metasurfaces may create further opportunities for encrypting sequences of images at different wavelengths for single-photon communication channels and the diversity of metasurface designs also opens up the possibility of spatially multiplexed imaging systems which, when combined with time-resolved imaging, can be used for quantum state tomography and exploration of entangled states with imaging techniques. Specifically, this work can be used to build on that demonstrated by Wang *et al.* [29] whereby a metasurface was designed and fabricated for the purpose of reconstructing the density matrix of a two-photon polarization state. This work required the use of pairs of single-pixel detectors to perform many two-photon correlation measurements, and the number of individual measurements performed could be reduced using the imaging capabilities presented in this Rapid Communication. This becomes particularly advantageous when extending the process to higher-dimensional states as discussed in Ref. [29].

The authors thank Prof. N. Zheludev for fruitful discussions. The authors acknowledge the support of the the support of the Singapore MOE Grants No. MOE2011-T3-1-005 and No. MOE2016-T3-1-006, ASTAR QTE Programme Grant No. SERC A1685b0005, EPSRC (U.K.) Grants No. EP/M009122/1 and No. EP/J00443X/1, and EU Grant No. ERC GA 306559. C.A. acknowledges the Robert A. Welch Foundation (Grant No. A-1943-20180324) and the Bio-Photonics initiative of the Texas A&M University. J.S.B. would like to thank the Robert A. Welch Foundation (Grant No. A-1261), Office of Naval Research (Award No. N00014-16-1-3054), and Air Force Office of Scientific Research (FA9550-18-1-0141). for their support.

[1] A. N. Boto, P. Kok, D. S. Abrams, S. L. Braunstein, C. P. Williams, and J. P. Dowling, Phys. Rev. Lett. **85**, 2733 (2000).
[2] M. D'Angelo, M. V. Chekhova, and Y. Shih, Phys. Rev. Lett. **87**, 013602 (2001).
[3] E. Brambilla, L. Caspani, O. Jedrkiewicz, L. A. Lugiato, and A. Gatti, Phys. Rev. A **77**, 053807 (2008).
[4] G. Brida, M. Genovese, and I. R. Berchera, Nat. Photonics **4**, 227 (2010).
[5] T. B. Pittman, Y. H. Shih, D. V. Strekalov, and A. V. Sergienko, Phys. Rev. A **52**, R3429(R) (1995).
[6] D. V. Strekalov, A. V. Sergienko, D. N. Klyshko, and Y. H. Shih, Phys. Rev. Lett. **74**, 3600 (1995).
[7] C. H. Monken, P. H. Souto Ribeiro, and S. Pádua, Phys. Rev. A **57**, 3123 (1998).
[8] J. H. Shapiro and R. W. Boyd, Quantum Inf. Process. **11**, 949 (2012).
[9] M. J. Padgett and R. W. Boyd, Philos. Trans. R. Soc. A **375**, 20160233 (2017).
[10] G. B. Lemos, V. Borish, G. D. Cole, S. Ramelow, R. Lapkiewicz, and A. Zeilinger, Nature (London) **512**, 409 (2014).
[11] R. S. Bennink, S. J. Bentley, and R. W. Boyd, Phys. Rev. Lett. **89**, 113601 (2002).
[12] A. Gatti, E. Brambilla, M. Bache, and L. A. Lugiato, Phys. Rev. Lett. **93**, 093602 (2004).
[13] J. H. Shapiro, D. Venkatraman, and F. N. C. Wong, Sci. Rep. **5**, 1 (2015).
[14] J. H. Shapiro, Phys. Rev. A **78**, 061802 (2008).
[15] B. Sun, M. P. Edgar, R. Bowman, L. E. Vittert, S. Welsh, A. Bowman, and M. J. Padgett, Science **340**, 844 (2013).
[16] A. Kirmani, D. Venkatraman, D. Shin, A. Colaço, F. N. C. Wong, J. H. Shapiro, and V. K. Goyal, Science **343**, 58 (2014).
[17] P. Ryczkowski, M. Barbier, A. T. Friberg, J. M. Dudley, and G. Genty, Nat. Photonics **10**, 167 (2016).
[18] E. Altewischer, M. P. van Exter, and J. P. Woerdman, Nature (London) **418**, 304 (2002).
[19] R. W. Heeres, L. P. Kouwenhoven, and V. Zwiller, Nat. Nanotechnol. **8**, 719 (2013).
[20] T. Roger, S. Vezzoli, E. Bolduc, J. Valente, J. J. F. Heitz, J. Jeffers, C. Soci, J. Leach, C. Couteau, N. I. Zheludev, and D. Faccio, Nat. Commun. **6**, 7031 (2015).
[21] S. Huang and G. S. Agarwal, Opt. Express **22**, 20936 (2014).
[22] C. Altuzarra, S. Vezzoli, J. Valente, W. Gao, C. Soci, D. Faccio, and C. Couteau, ACS Photonics **4**, 2124 (2017).
[23] T. Roger, S. Restuccia, A. Lyons, D. Giovannini, J. Romero, J. Jeffers, M. Padgett, and D. Faccio, Phys. Rev. Lett. **117**, 023601 (2016).
[24] B. Vest, M. C. Dheur, É. Devaux, A. Baron, E. Rousseau, J. P. Hugonin, J. J. Greffet, G. Messin, and F. Marquier, Science **356**, 1373 (2017).
[25] W. T. Chen, K.-Y. Yang, C.-M. Wang, Y.-W. Huang, G. Sun, I.-D. Chiang, C. Y. Liao, W.-L. Hsu, H. T. Lin, S. Sun, L. Zhou, A. Q. Liu, and D. P. Tsai, Nano Lett. **14**, 225 (2014).

[26] D. Wen, F. Yue, G. Li, G. Zheng, K. Chan, S. Chen, M. Chen, K. F. Li, P. W. H. Wong, K. W. Cheah, E. Yue Bun Pun, S. Zhang, and X. Chen, Nat. Commun. **6**, 8241 (2015).

[27] X. Yin, M. Schäferling, B. Metzger, and H. Giessen, Nano Lett. **13**, 6238 (2013).

[28] T. Stav, A. Faerman, E. Maguid, D. Oren, V. Kleiner, E. Hasman, and M. Segev, Science **361**, 1101 (2018).

[29] K. Wang, J. G. Titchener, S. S. Kruk, L. Xu, H.-P. Chung, M. Parry, I. I. Kravchenko, Y.-H. Chen, A. S. Solntsev, Y. S. Kivshar, D. N. Neshev, and A. A. Sukhorukov, Science **361**, 1104 (2018).

[30] T. Kim, M. Fiorentino, and F. N. C. Wong, Phys. Rev. A **73**, 012316 (2006).

[31] A. Fedrizzi, T. Herbst, A. Poppe, T. Jennewein, and A. Zeilinger, Opt. Express **15**, 15377 (2007).

[32] All data are available at DOI: http://dx.doi.org/10.5525/gla.researchdata.704.